KaMLs for Predicting Protein pK_a Values and Ionization States: Are Trees All You Need?

Mingzhe Shen,[†] Daniel Kortzak,[†,§] Simon Ambrozak,[‡] Shubham Bhatnagar,[‡] Ian Buchanan,[¶] Ruibin Liu,[†] and Jana Shen[*,†]

† *Department of Pharmaceutical Sciences, University of Maryland School of Pharmacy, Baltimore, MD 21201*
‡ *Department of Computer Science, University of Maryland College Park, College Park, MD 20742*
¶ *Stuyvesant High School, New York, NY 10282*
§ *Joint first author*

E-mail: jana.shen@rx.umaryland.edu

Abstract

Despite its relevance for understanding biology and computer-aided drug discovery, accurate prediction of protein ionization states remains a formidable challenge. Physics-based approaches struggle to capture the small, competing contributions in the complex protein environment, while machine learning (ML) is hampered by scarcity of experimental data. Here we developed the pK_a ML (KaML) models based on decision trees and graph attention networks (GATs), exploiting physicochemical features and a new experiment pK_a database (PKAD-3) enriched with highly shifted pK_a's. KaML-CBtree significantly outperforms the current state of the art in predicting pK_a values and ionization states across all six titratable amino acids, notably achieving accurate predictions for deprotonated cysteines and lysines – a blind spot in previous models. The superior performance of KaMLs is achieved in part through several innovations, including separate treatment of acid and base, utilization of pK_a shifts as training targets, data augmentation using AlphaFold structures, and model pre-training on a theoretical pK_a database. A meta-feature analysis reveals why the lightweight tree model outperforms the more complex deep learning GAT. We release an end-to-end pK_a predictor based on KaML-CBtree and the new database PKD-3, enabling applications and laying groundwork for further advances in protein electrostatics research.

INTRODUCTION

Ionizable residues in proteins play a variety of roles in biology. For example, enzyme reactions often involve catalytic acid and base which can donate or abstract a proton,[1] while pH-dependent ion channels and transporters sense the pH gradient through protonation or deprotonation of gating residues.[2,3] Redox processes often involve a reactive Cys that is either deprotonated or has a high tendency to deprotonate at physiological pH.[4] Ionizable residues offer unique opportunities for targeted covalent drug discovery. In particular, deprotonated Cys and Lys residues are nucleophilic, making them valuable targets for covalent inhibitors.[5] Protein ionization equilibria are characterized by the pK_a values, which may significantly deviate from the solution (model) values. Thus, knowledge of protein pK_a values is important.

Solution NMR is the method of choice for site-specific pK_a determination;[6] however, it is costly and time-consuming. Computational methods offer a potential alternative; however, achieving accuracy and efficiency in pK_a calculations remains a formidable challenge.[7] Several physics-based pK_a prediction approaches have been developed in the past.[7] A classic approach is based on solving the Poisson-Boltzmann (PB) equation; popular software tools include H++,[8] DelPhiPKa,[9] PDB2PQR,[10] MCCE2,[11] and PypKa.[12] One major limitation is the assumption of a uniform protein dielectric constant. In reality, this constant varies from the interior to the surface of the protein.[13] Significantly faster than PB solvers are empirical methods based on energy functions, e.g., the popular PROPKA program[14,15] calculates the pK_a shifts relative to the model values using contributions from desolvation, hydrogen-bonding (h-bond), and charge-charge interactions. Arguably the most accurate and most time consuming pK_a calculation method[7] is based on constant pH molecular dynamics (MD) simulations,[16] e.g., the generalized Born (GB) based[17] or all-atom particle Ewald continuous constant pH MD (CpHMD).[18]

In recent years, machine learning (ML) models for pK_a predictions have emerged as an alternative to physics-based approaches; however, building ML pK_a predictors is challenging due to the lack of experimental data. Alexov and coworker spearheaded the effort to curate experimental pK_a's and published the first database PKAD,[19] which was recently expanded to PKAD-2.[20] PKAD-2 contains 1,742 entries; however, due to the inclusion of multiple protein data bank (PDB) structures per protein and/or multiple pK_a measurements per residue, these entries correspond to only 615 unique residues in 113 unique wild-type (WT) or mutant proteins (Table 1). Moreover, the majority of pK_a's belong to Asp (175), Glu (218), and His (116), while only 20 Cys, 19 Tyr, and 67 Lys are included (Table 1). Furthermore, most of the pK_a's cluster around the model values and significantly shifted pK_a's are rare (Figure 1A), making it challenging to train ML models capable of predicting large pK_a shifts which are often crucial for biological functions.

To tackle data scarcity, Reis, Machuqueiro et al. developed pKPDB,[21] a theoretical pK_a database comprised of 12 million pK_a's of six titratable amino acids calculated using PypKa,[12] a Python API for the fast PB solver DelPhi v5.[22] Based on pKPDB, Reis, Machuqeiro, Clevert et al. trained PKAI+ (a multilayer perceptron),[23] which achieved root-mean-square error (RMSE) of 0.98 on a subset of 750 pK_a's from the PKAD database.[19] Using pH replica-exchange[24] GBNeck2-CpHMD titration simulations,[25,26] Huang and coworkers created a theoretical database PHMD549[27] comprising 27k pK_a's of Asp, Glu, His, and Lys from 549 proteins. A convolutional neural network (CNN) DeepKa[27] trained on PHMD549 achieved RMSE of 0.96 and Pearson's correlation coefficient (PCC) of 0.74 when evaluated on 167 pK_a's from PKAD.[19]

Recently, ML models trained on experimental pK_a data have also been reported. Based on PKAD[19] and 23 additional mutant pK_a's, Chen, Lee, Damjanovic et al. trained decision tree models using 12 features.[28] After correcting for training/test data leakage, the RMSE of the best model XGBoost is above 1 (Damjanovic, Protein Electrostatics Conference 2023, Genoa, Italy). Based on PKAD,[19] Yang, Luo and coworker[29] trained XGBoost tree model using atom-based as well as distance features, which gave RMSE of 1.0 for Asp, Glu, His, and Lys when evaluated on 20% of the unseen PKAD data. Using ANI-2x atomic environment vector embedding, Isayev and coworker developed neural networks for individual titratable amino acids. Training on a subset of PKAD,[19] ANI-2x[30] achieved RMSEs of 0.59 (Glu), 0.94 (Asp), and 0.98 (His) in one hold-out test.

Building on recent advances, this work addresses key challenges in pK_a predictions. First, we developed a new database PKAD-3, which expands upon and refines PKAD-2.[20] Next, we developed p$\boldsymbol{K_a}$ **M**achine **L**earning models (KaMLs), using the CatBoost deci-

sion tree (CBtree) model and graph attention network (GAT),[31] for protein pK_a predictions. KaML-CBtree and KaML-GAT achieve state-of-the-art performance through several innovations, such as the separate treatment of acidic and basic residues; incorporation of features representative of pK_a determinants; utilization of pK_a shifts as training targets; data augmentation with AlphaFold2 (AF2) structures;[32] and model pre-training on a theoretical pK_a database.

To enhance practical relevance, we extended our model evaluation to include metrics for protonation state predictions. Additionally, in contrast to the previous publications, we implemented rigorous data splitting to prevent data leakage and evaluated models 20 times to offer statistical uncertainties of model performance. We then benchmarked the KaMLs against the baseline models (null model and PROPKA3[15]) and the PB solver (PypKa[12]) as well as two different types of ML models (DeepKa[27] and ANI-2X[30]). Finally, using meta-feature analysis we rationalized the superior performance of the light-weight KaML-CBtree over the more complex KaML-GAT.

Results and Discussion

Development of PKAD-3 and analysis of experimental pK_a values

Developing an expanded, high-quality experimental pK_a database PKAD-3. An extensive and high-quality dataset is of utmost importance for training and testing ML models. Following manual verification and error correction of entries in PKAD-2,[20] a literature search for additional experimental pK_a values was conducted. We refer to the expanded database as PKAD-3, in tribute to the pioneering efforts of the Alexov group.[19,20] PKAD-3 contains 1167 pK_a's of 992 unique residues in 247 proteins (WT or mutant), representing increases of 53%, 61%, and 119% over the corresponding numbers (763 pK_a's of 615 residues in 113 proteins) in the cleaned-up PKAD-2 (Table 1). Note, since some residues and pK_a's are associated with more than one PDB structure, PKAD-2 contains a total of 1286 PDB entries, which was mistakenly cited as the number of pK_a's in the previous publications.[20,23,28–30] To facilitate community efforts in developing pK_a prediction tools, we implemented PKAD-3 as a freely searchable and downloadable web database (`http://database.computchem.org/pkad3`).

Analyzing experimental pK_a distributions of six titratable amino acids. Compared to PKAD-2, there is a substantial increase in the number of (unique) residues with experimental pK_a's for all six titratable amino acids, particularly Cys and Tyr (Table 1 and Figure 1A). The number of Cys and Tyr increases by 185% (from 20 to 57) and 100% (from 19 to 38), respectively. The number of Asp, Glu, and Lys increases by 58–67%, while the number of His shows a modest increase of 34%. As in PKAD-2, the number of residues and experimental pK_a's for Glu, Asp, His, Lys, Cys, and Tyr follows a descending order (Table 1).

Before training ML models, it is instructive to examine the distributions of target data (Figure 1A). The pK_a distributions of individual amino acids exhibit distinct patterns. His pK_a's display a nearly Gaussian distribution centered around the model pK_a of 6.5, demonstrating that His can be protonated, deprotonated, or titrating at physiological pH. This also suggests that allowing His titration in MD simulations via constant pH techniques[16] may be necessary.

Cys pK_a's exhibit a distinctive bimodal distribution with two peaks of similar heights. Surprisingly, the major peak is near pK_a 5—6, indicating deprotonation at physiological pH. Deprotonated Cys or those with pK_a's near physiological pH are referred to as hyperreactive or reactive, as they are prone to chemical modifications and play important roles in catalysis and redox chemistry.[4,17,33] The secondary peak of Cys pK_a's is located at 9–10, indicating protonation at physiological pH. The unique pK_a distribution of Cys, com-

Table 1: Statistics[a] of pK_a databases PKAD-2 and PKAD-3

	PKAD-2[b]			PKAD-3			% incr.		
	Res	pK_a's	PDBs	Res	pK_a's	PDBs	Res	pK_a's	PDBs
Asp	175	214	403	291	330	520	66.3%	54.2%	29.0%
Glu	218	258	447	342	382	580	56.9%	48.1%	29.8%
His	116	170	243	155	219	293	33.6%	28.8%	20.6%
Cys	20	20	20	57	60	62	185.0%	200%	210%
Tyr	19	20	22	38	39	41	100.0%	95.0%	86.4%
Lys	67	81	151	109	137	216	62.7%	69.1%	43.0%
Total	615	763		992	1167		61.3%	52.9%	
Entries			1286			1712			33.1%
Proteins			113			247			118.6%

[a]The number of unique residues, the number of measured pK_a's, the number of PDB entries (X-ray structures), and the number of unique wild-type or mutant proteins. The number of PDBs includes several modeled structures for mutant proteins. [b]A cleaned-up version of PKAD-2,[20] where pK_a's given in ranges were removed and errors were corrected (see Methods).

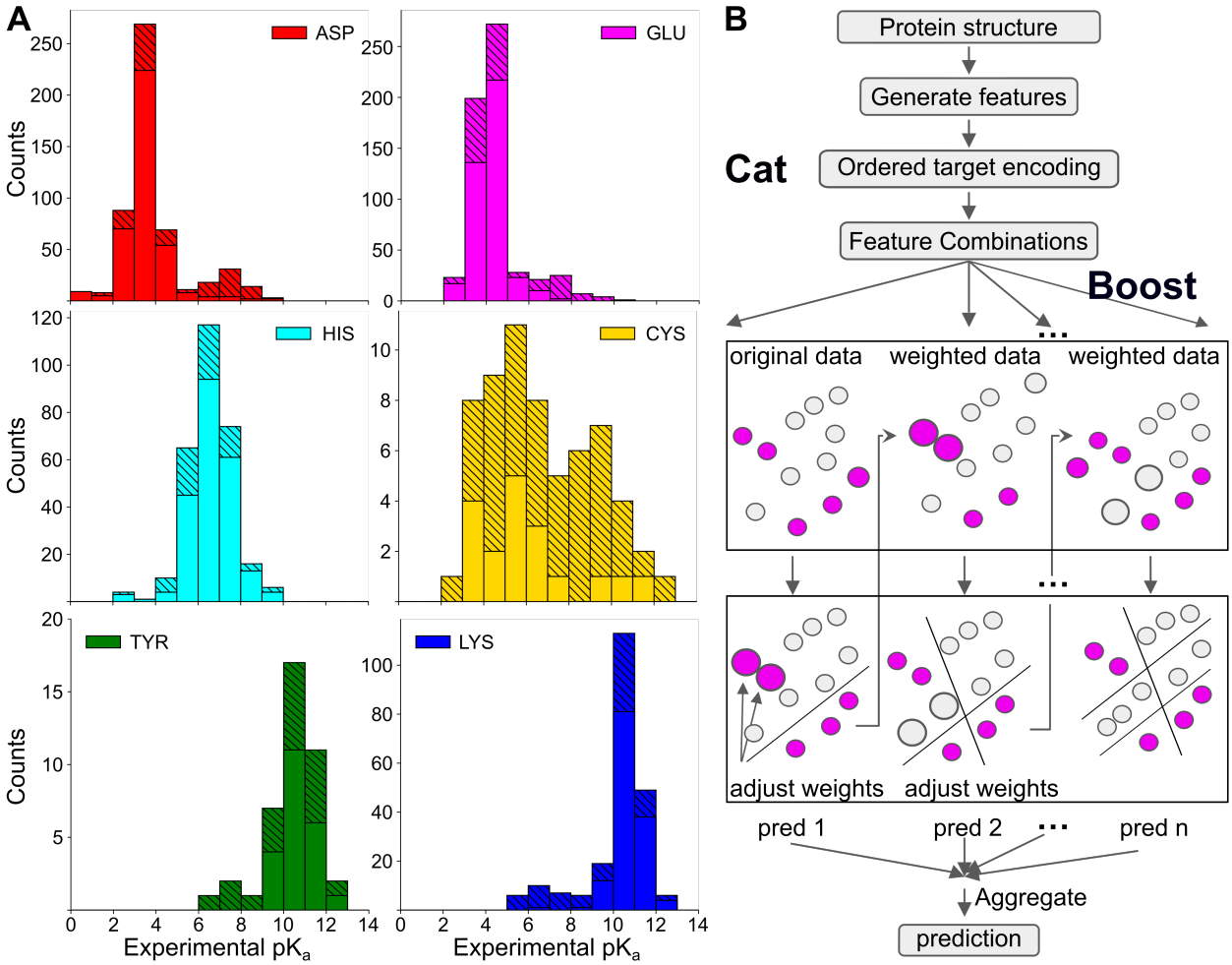

Figure 1: **Overview of the pK_a dataset and illustration of KaML-CBtree. A.** Histograms of the experimental pK_a values in PKAD-3 database. Solid bars represent the data in the cleaned PKAD-2 database and striped bars represent the data added in this work. **B.** The Catboost algorithm. CatBoost handles categorical features using ordered target statistics to capture the relationship with the target variable. Gradient boosting algorithms sequentially build an ensemble of decision trees, where each tree corrects the errors of the previous ones by adjusting the weights for data points with large prediction errors. The final aggregated prediction is the sum of the individual predictions of all trees.

bined with the small dataset, presents a challenge for ML models. The prevalence of deprotonated Cys suggests a potential source of inaccuracy in MD simulations, as protonated form is the default state.

The pK_a distributions of Asp, Glu, Tyr, and Lys are bimodal, with a dominant peak near the model pK_a and a minor peak at a higher (Asp and Glu) or lower (Tyr and Lys) pK_a's. The pK_a ranges of Asp and Glu extend up to approximately 9, demonstrating that Asp and Glu can titrate or even protonate at physiological condition. Most of these large pK_a's were obtained by the García-Moreno lab through NMR or denaturation experiments of the engineered mutants of staphylococcal nuclease (SNase), whereby a buried hydrophobic residue is replaced with a titratable one.[34–36]

The mutant SNase experiments also contributed Lys pK_a's that extend down to values as low as 5,[37,38] indicating that Lys can titrate or deprotonate at physiological condition. In addition to producing large pK_a shifts, some of the mutated residues in SNase show normal (i.e. near model) pK_a's despite being buried in the interior.[39] These normal and significantly shifted pK_a's are collectively termed anomalous pK_a's; they provide crucial training data for ML models to generalize across diverse protein environments and capture rare but functionally relevant pK_a's. Note, anomalous pK_a's are most challenging to predict accurately using physics-based approaches[7] and may require accurate description of ionization-induced conformational changes.[39]

Similar to Lys but to a smaller extent, the pK_a distribution of Tyr displays low values of 6–9, indicating that some Tyr can titrate or even deprotonate at physiological pH. Due to the extremely small dataset, it is challenging to train ML models that can predict deprotonated Tyr.

Training and evaluating KaML-trees

Feature engineering and visualization. Due to the small dataset (1,167 pK_a's in PKAD-3), we first turned to the "shallow learning" tree models, which recursively divide features into subsets, forming a tree-like structure of decisions. We adapted our recent tree features for predicting Cys ligandabilities,[40] which include three types of numerical features representing the physical determinants of pK_a shifts:[15,35,41] solvent accessibility, potential hydrogen bonding, and electrostatic interactions. Additionally, categorical features that describe residue type, net charge, and secondary structures in proximity to the titratable residue were included (see complete list in Methods and SI Table S1.

To test if the tree features exhibit clusters that are correlated with protonation states, we employed t-distributed stochastic neighbor embedding (t-SNE) algorithm,[42,43] which calculates pairwise similarities between data points in the high-dimensional space and maps them to a lower-dimensional space while preserving the neighbor identities.[42,43] His pK_a's are clustered near 7, and therefore we used their features as a stringent test case. Using t-SNE, the 37 numerical features are mapped on two dimensions, where each point is colored by the (target) protonation state (Figure 2 for pH 7 and SI Figure S2 for pH 7.5). The plot displays several clusters, each predominantly characterized by a single color, suggesting that the features can effectively discriminate between distinct protonation states.

Data splitting, training and evaluating the acid and base KaML-trees. We separated the data into acidic (Asp, Glu, Cys, Tyr) and basic (His and Lys) residues due to the distinct mechanisms of pK_a shifts and trained separate models for them (see later discussion). This resulted in 728 acidic residues (811 pK_a's and 1203 PDB entries) and 264 basic residues (356 pK_a's and 509 PDB entries). The data was randomly split into 90% for training and 10% for hold-out test. To prevent data leakage, splitting was based on unique residues and stratification was applied based on the pK_a's (details see Methods). Ini-

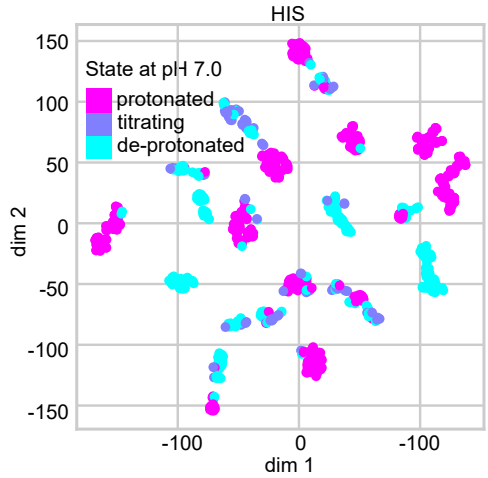

Figure 2: **t-SNE visualization of the histidine features.** The 37 numerical features of His were extracted from the dataset with the AF2 augmentation and mapped on two dimension using t-SNE. The color code indicates the protonation state at pH 7 based on the label (experimental) pK_a: deprotonated (p$K_a > 7.48$); protonated (p$K_a < 6.52$); and titrating ($6.52 \leq$ p$K_a \leq 7.48$).

tially, five types of tree models were trained: Random forest (RF), Extra trees (ET), gradient boosting (GB), extreme gradient boosting (XGB) and Catboost (CB). Each model was trained on each of the 20 different train/test splits and 10 fold cross-validation (CV) was used during training. Mean square error (MSE) of pK_a's was used as training loss. The average and standard deviation of PCC, RMSE, and absolute maximum error (MAXE) from 20 hold-out tests were used as evaluation metrics.

We first compared the metrics of the different tree models (SI Table S2). Considering all residues, the PCCs of all five tree models are nearly identical (0.94); however, the CBtree yields the lowest RMSE (0.77) and MAXE (3.47), followed by ETtree, which yields RMSE of 0.80 and MAXE of 3.70. Considering acid and base separately, the acid CBtree remains the best, with the RMSE of 0.77 and MAXE of 3.25, as compared to 0.82 and 3.61 with the ETtree, although the RMSE and MAXE of the base CBtree (0.76 and 2.60) are slightly higher than those of the base ETtree (0.74 and 2.46).

For practical applications, the exact pK_a is often less relevant than the protonation state at a specific pH, e.g., the physiological cytosolic pH of 7.1. Thus, we evaluated the model's performance of correctly predicting protonation states by discretizing the predicted pK_a's in three classes based on the protonation probability (Prob) at pH 7: protonated ($\mathrm{Prob} > 0.75$ or p$K_a < 6.52$), deprotonated ($\mathrm{Prob} < 0.25$ or p$K_a > 7.48$), or titrating ($0.25 \leq \mathrm{Prob} \leq 0.75$ or $6.52 \leq$p$K_a \leq 7.48$). This discretization step effectively transforms the regression problem into a classification task, and consequently, the models can be evaluated by the class precision (Pre) and recall (Rec).

Here we concern ourselves with the protonated and deprotonated classes and defer the discussion of the titrating class to future work. Rec informs the percentage of protonated (deprotonated) residues identified, while Pre informs the correct percentage of the identified protonated (deprotonated) residues. Since incorrectly predicting protonated as deprotonated or vice-versa is the most consequential error, we evaluated the percentage of these "misclassified" instances and referred to it as critical error rate (CER).

Considering Pre/Rec for protonated and deprotonated classes of all residues (SI Table S3), the CBtree again emerged as the the best performing tree model, yielding Pre/Rec of $0.97/0.93$ for protonated class and $0.94/0.94$ for deprotonated class (SI Table S3). The CER of CBtree is also the lowest (46/2635). Considering Pre/Rec and CER of the acid and base models separately (Table 2), the CER of the base CBtree is nearly three times lower than ETtree, although the acid CBtree has slightly lower Rec and higher CER than the acid ETtree. Since CBtree has overall the best performance, we will drop the other tree models in the remainder of the discussion.

KaML-CBtree outperforms PROPKA3 in pK_a prediction accuracy across all titratable amino acids. The CBtree significantly outperforms the baseline models, PROPKA3[15] and null model, in pK_a predic-

Table 2: Performance metrics of KaML-CBtree for acid and base pK_a and protonation state predictions in comparison to the baseline models[a]

	KaML-CBtree		KaML-GAT	PROPKA3		Null	
	acid	base	acid + base	acid	base	acid	base
PCC	0.88 ± 0.03	0.92 ± 0.03	0.93 ± 0.02	0.74 ± 0.06	0.90 ± 0.04	0.55 ± 0.06	0.86 ± 0.04
RMSE	0.76 ± 0.13	0.79 ± 0.10	0.90 ± 0.08	1.28 ± 0.15	0.96 ± 0.18	1.36 ± 0.11	1.04 ± 0.10
MAXE	3.17 ± 0.61	2.60 ± 0.70	3.74 ± 0.49	3.72 ± 0.29	5.04 ± 0.46	5.55 ± 1.24	2.80 ± 0.67
Classification of protonation states at pH 7[b]							
Pre (prot)	0.91	0.99	0.92	0.66	0.97	0.63	0.97
Rec (prot)	0.82	0.97	0.92	0.78	0.88	0.39	0.78
Pre (dep)	0.99	0.95	0.98	0.98	0.97	0.95	0.77
Rec (dep)	0.99	0.99	0.98	0.97	0.85	0.98	0.97
CER[c]	34/2099	12/536	70/2822	90/2055	53/618	141/2106	101/716

[a]Baseline models include PROPKA3[15] and null model which returns the model pK_a's:[44] 3.7 for Asp, 4.2 for Glu, 6.5 for His, 8.5 for Cys, 9.5 for Tyr, and 10.4 for Lys. [b]Prediction is based on the probability of protonation given a predicted pK_a (see main text). [c]Critical error rate (CER) refers to the percentage of miss-classifying protonated as deprotonated or vice versa. All classification metrics were calculated after accumulating the predictions from all 20 hold-out test sets.

tions. The CBtree yields PCCs of 0.88/0.92, RMSEs of 0.76/0.79, and MAXEs of 3.17/2.60 for acid/base residues, as compared to PROPKA3's PCCs of 0.74/0.90, RMSEs of 1.28/0.95, and MAXEs of 3.72/5.04 (Table 2). Importantly, the differences between CBtree and PROPKA3 far exceed the statistical uncertainties of the model evaluations.

Amino acid specific PCC is a stringent evaluation metric due to the narrow pK_a range for individual amino acids. The CBtree yields PCCs of 0.86 for Asp, 0.84 for Glu, 0.51 for His, 0.61 for Cys, and 0.80 for Lys, which are higher than PROPKA3's PCCs of 0.64 for Asp, 0.69 for Glu, 0.45 for His, 0.12 for Cys, and 0.75 for Lys (Figure 3A). The most notable improvement is for Cys, as PROPKA3 predictions do not offer statistically meaningful correlation with experiment, which is likely due to the extremely small number of experimental Cys pK_a's used in fitting the PROPKA3 model.[15]

Comparing the CBtree PCCs across different amino acids, Asp, Glu, and Lys show the highest PCCs around 0.8, whereas the PCCs for His and Cys are much lower, 0.51 and 0.61, respectively. The low PCC for His may be attributed to its narrow pK_a distribution (Figure 1A), in which case even small errors can decrease the PCC.

Compared to PROPKA3 and null model, the CBtree's RMSEs are lower for all six amino acids (Figure 3A and B). The CBtree yields RMSEs of 0.75 for Asp, 0.60 for Glu, 0.85 for His, 1.50 for Cys, 1.24 for Tyr, and 0.70 for Lys, which are significantly lower than PROPKA3's RMSEs of 1.12 for Asp, 1.02 for Glu, 1.03 for His, 3.58 for Cys, 1.67 for Tyr, and 0.80 for Lys. The largest RMSE reduction is for Cys, 2.1. In contrast, the smallest RMSE reduction is for His, only 0.18, which is due to the concentration of experimental pK_a values around the model value (Figure 1A). This is supported by the RMSE of null model being 0.06 lower than PROPKA3 (Figure 3A).

Comparing the CBtree's RMSEs across different amino acids, Glu shows the smallest RMSE of 0.60, which approaches the experimental pK_a error of 0.5 units.[6] This level of accuracy likely stems from the extensive training dataset (580 pK_a's of 342 residues; Table 1). The largest RMSE is for Cys (1.50), followed by Tyr (1.24; Figure 3A). This trend is the same for both the CBtree and PROPKA3, reflecting the small size of training or fitting (in the case of PROKA3) dataset.

KaML-CBtree outperforms PROPKA3 in protonation state classification across all six amino acids. Considering acid and base separately, CBtree yields higher Pre

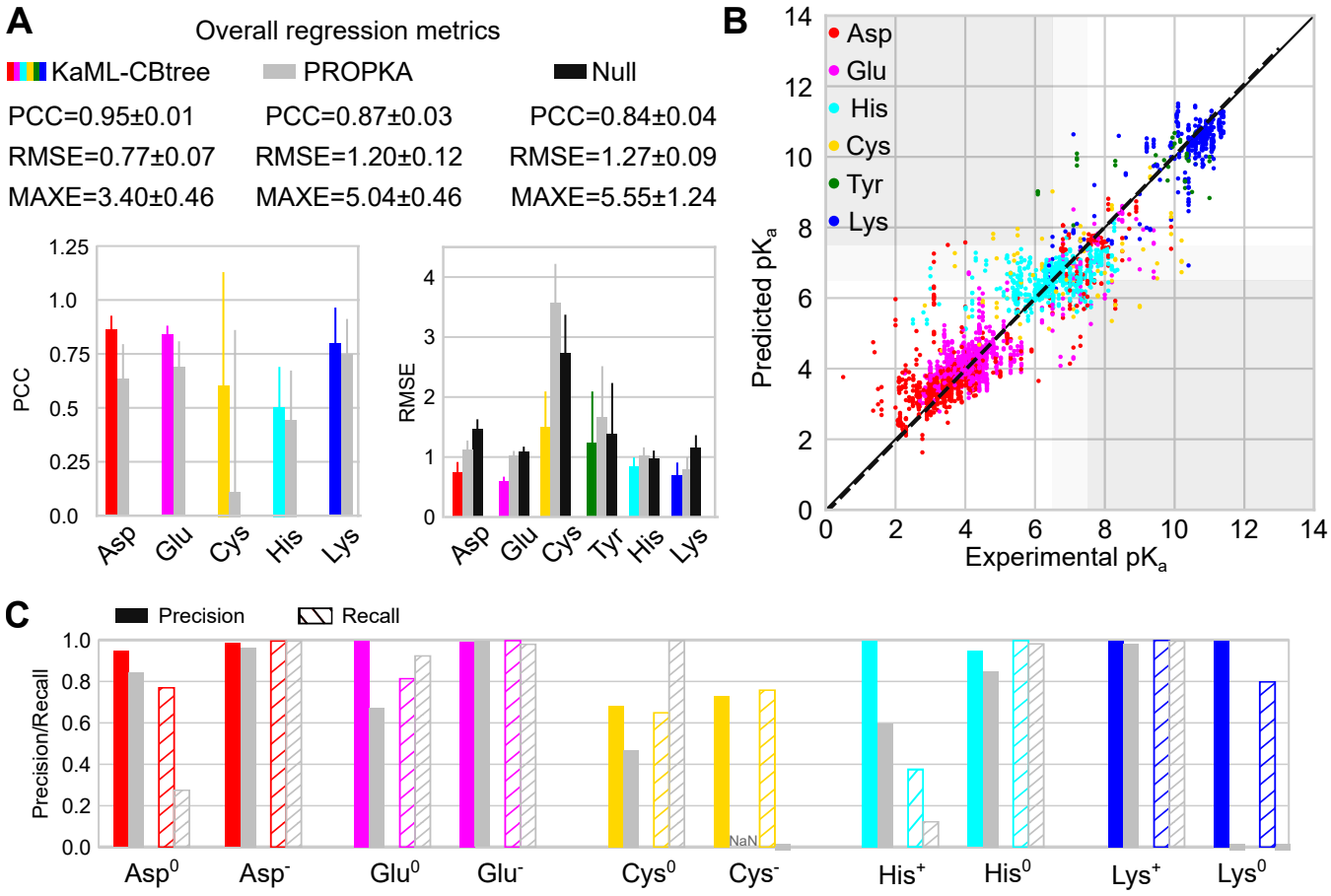

Figure 3: **Evaluation of KaML-CBtree for predicting pK_a's and protonation states of individual titratable amino acids. A.** Top. Overall performance metrics of KaML-CBtree (color-coded), PROPKA3 (grey), and null model (black). Bottom. PCC and RMSE for individual amino acids. The mean and SD of 20 hold-out tests are given. **B.** Experimental vs. predicted pK_a's from all 20 test sets (see SI Figure S3 for plots of individual test sets). The solid line is the identity and the dotted line is a linear fit. Data points are color-coded by amino acid. The white regions indicate correct protonation state classifications. The dark gray regions highlight the critical errors. The light gray regions indicate titrating pK_a's which were excluded from the classification analysis. **C.** The precision (solid) and recall (with stripes) of classifying protonated and deprotonated amino acids at pH 7 using KaML-tree (color-coded) and PROPKA3 (grey).[15] PROPKA3 fails to predict any Cys^-; thus precision is undefined (NaN). Classification analysis for Tyr is not shown due to the extremely small test sets.

and Rec of both protonated and deprotonated states than PROPKA3 and null model in (Table 2). The most dramatic improvement is in the reduction of CER. CBtree's CER in predicting acid protonation states is 34/2099, which is nearly three times lower than PROPKA3 (90/2055) and more than four times lower than null model (141/2106). CBtree's CER in predicting base protonation states is 12/536, which is more than four times lower than PROPKA3 (53/618) and more than ten times lower than null model (101/716). For acids, the drastic reduction in CER can be largely attributed to the more precise prediction of protonated acids (Pre of 0.91 for CBtree vs. 0.66 for PROPKA3 and 0.63 for null model). For base, the reduction in CER can be attributed to the higher recall of both protonated and deprotonated base residues.

Dramatic improvement in predicting Asp^0, Glu^0, Cys^-, and Lys^0. We compare CBtree's protonation state classification for individual amino acids with PROPKA3 (Figure 3C and SI Table S4 and S5). Null model is not evaluated, because it predicts only one state. We first consider acids, Asp, Glu, and Cys. Since Asp^- and Glu^- are dominant, both the CBtree and PROPKA have high Pre/Rec; however, the CBtree has a better performance for predicting Asp^0 and Glu^0. In particular, CBtree's Rec for Asp^0 (0.77) exceeds PROPKA3's (0.28) by nearly 0.5, and CBtree's Pre for Glu^0 (1.0) exceeds PROPKA3's (0.67) by 0.33. Significantly, CBtree's Pre/Rec for Cys^- is 0.73/0.76, whereas PROPKA3 fails to identify any Cys^-, instead assigning Rec of 1 for Cys^0.

For base amino acids (His and Lys), CBtree shows the most dramatic improvement in predicting Lys^0, achieving Pre/Rec of 1.0/0.8, while PROPKA3 fails to identify any. His protonation state at pH 7 is most challenging to predict, due to most pK_a's concentrating around 6.5. While both models have high Pre/Rec for His^0, the CBtree predicts His^+ with Pre/Rec of 1.0/0.37, as compared to PROPKA3's 0.60/0.12. Note, the recall appears very low; however, due to class imbalance the recall from random guess is only 0.24. Finally, CBtree's CERs are 2.4–6 times lower than PROPKA3's across five titratable amino acids: 13/31 for Asp, 5/21 for Glu, 11/47 for His, 13/35 for Cys, and 1/6 for Lys.

Why does training separate acid and base KaML-CBtrees boost performance? To understand the necessity of training separate tree models for acid and base residues, we examine the feature impacts in the SHapley Additive exPlanations (SHAP)[45] plots for the unseen tests (Figure 4). As expected, the model pK_a makes the largest impact in both acid and base pK_a predictions. The next largest contributing features, however, impact the acid and base pK_a predictions differently. In acid pK_a predictions, a high buried_ratio shifts the SHAP value and predicted pK_a up, increasing the probability of protonation. A similar impact is made by increasing the number of polar side-chains within 10 Å around the residue of interest (n_polar10). Similar to buried_ratio and n_polar10, the number of polar side-chains within 15 Å (n_polar15) is the second largest contributor in base pK_a predictions; however, increasing its value shifts the SHAP value and predicted pK_a down, increasing the probability of deprotonation.

Impacts of opposite signs are also made by features representing attractive electrostatic interactions. In acid pK_a predictions, decreasing the distance to the nearest His side-chain nitrogen (d0_hbond_h) downshifts the SHAP value and pK_a, increasing the probability of deprotonation. In base pK_a predictions, decreasing the distance to the nearest negatively charged oxygen (d0_neg_O) upshifts the SHAP value and pK_a, increasing the probability protonation.

The above analysis demonstrates that although important features are shared between acid and base pK_a predictions, the impacts on pK_a predictions are in opposite directions. This explains why training separate acid and base KaML-trees offers a significant performance boost.

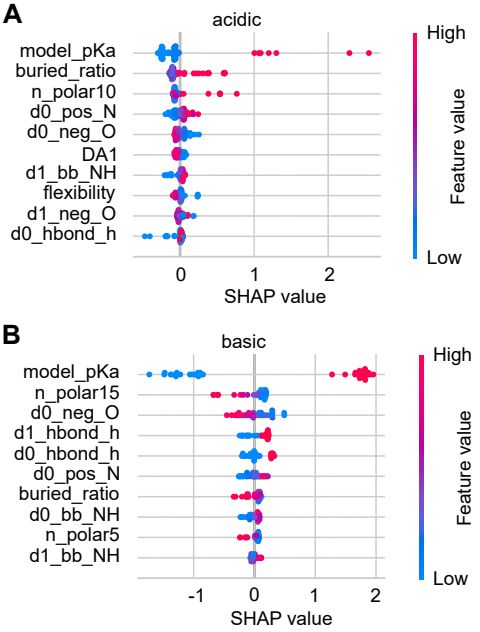

Figure 4: **Impacts of features on the pK_a predictions of acid and base residues.** SHAP value plots for the acid (**A**) and base (**B**) pK_a predictions. The top ten features with the largest average contributions are shown. Each data point is an instance in the test data. Feature values are colored from blue (low) to red (high). The position along the SHAP value axis shows how a feature value shifts the model output. An explanation of all features is given in SI Table S1.

Training and evaluating KaML-GAT

Building KaML-GATs, data augmentation and model pretraining. In an attempt to further improve the pK_a and protonation state predictions, we turned to GAT,[31] an improved version of convolutional graph neural network (GNN). A GNN is designed to process graph-structured data such as protein structures; through message passing steps, the information stored in nodes and edges (node and edge embeddings) can be exchanged with their neighbors. A GAT allows attention to be added based on the neighboring nodes' features, allowing more weights to be applied to important features. The KaML-GAT architecture and workflow are illustrated in Figure 5A. A graph was constructed for each titratable residue by truncating the protein structure using a 10-Å sphere centered at the center of mass of the titratable side-chain. Each node (atom) is represented by a 42-digit vector embedding, similar to the channels of the CNNs for Cys ligandability predictions.[40] A 24-digit one-hot encoding for the atom types was added (SI Table S6). The message passing is enabled through 3 one-head convolutional layers with 42 channels. Following a global average pooling layer, two hidden layers containing 32 and 16 neurons with a dropout rate of 0.2 are employed before a final layer that makes a pK_a prediction.

Deep learning requires a large amount of data. To tackle data shortage, we implemented a two-pronged approach: data augmentation to artificially expand the dataset, and model pre-training by leveraging a larger, related dataset. To augment data, we added (based on feature calculations at most 10) AlphaFold2 (AF2) structure models[32] for residues with an absolute pK_a shift greater than 2 (see Methods). As target labels, we used pK_a shifts (reduction in the average test RMSE by 0.3 compared to using pK_a's as labels, data not shown). Unlike KaML-trees, a single GAT outperformed separate acid and base models, yielding lower test RMSE. For model pre-training, we employed PHMD549, which contains GBNeck2-CpHMD calculated

pK_a's of Asp, Glu, His, and Lys.[27] After removing the residues in PKAD-3, this dataset contains 26,252 pK_a's of 25,912 residues in 535 proteins. Data splitting (9:1 ratio for train:test) and hold-out test sets are identical to those used for KaML-trees (SI Figure S1). In model pre-training, 10% of data was reserved for evaluation, i.e., model selection and hyperparameter tuning. The pre-trained model yields an RMSE of 0.79 for the validation data (SI Figure S4).

The fine-tuned ensemble KaML-GAT outperforms PROPKA3 and null model in overall metrics. Following pre-training on PHMD549, the GAT was fine-tuned by training on the AF2 augmented PKAD-3. Hold-out tests with 0, 1, or 2 frozen GAT layers demonstrated that releasing all layers gave the lowest overall RMSE and highest overall PCC (SI Table S7). We also tested the idea of aggregating multiple "weak predictors" to enhance performance.[46] Specifically, for each training set, 10 models were trained using 10 different training:validation (9:1 ratio) splits, and this process was repeated for each train:hold-out data splits (20 times total). The ensemble average RMSE decreases and plateaus as the model number reaches 8 (SI Figure S6). Thus, we further evaluated the 10-model based ensemble GAT. For simplicity, we drop the word ensemble in the remainder of the discussion.

The GAT outperforms PROPKA3 and null model in the overall PCC, RMSE, and MAXE (Table 2). The largest improvement is in RMSE/MAXE. The GAT yields RMSE/MAXE of 0.90/3.74, compared to 1.20/5.04 by PROPKA3 and 1.27/5.55 by null model. In classification of deprotonation states at pH 7, the GAT also outperforms PROPKA3 and null model. The largest improvement is in CER. Out of 2822 instances, GAT's CER is 70, which is twice and three times lower than PROPKA (143) and null model (242), respectively.

KaML-GAT outperforms PROPKA3 for Asp, Glu, and Cys but not for His, Lys and Tyr. The GAT more accurately predicts pK_a's for Asp, Glu, and Cys (Figure 5B and D and SI Table S8). The GAT's PCC/RMSE are 0.82/0.88 (Asp), 0.73/0.76 (Glu), and 0.59/1.81 (Cys), compared to PROPKA3's 0.64/1.12 (Asp), 0.69/1.02 (Glu), and 0.12/3.58 (Cys). The GAT yields significantly higher Rec (0.75) for Asp^0, compared to 0.28 with PROPKA3 (Figure 5D). As to Glu^0, the GAT gives a higher Pre (1.0), compared to 0.67 with PROPKA3; however, the GAT's Rec (0.52) is lower than that of PROPKA3 (0.93). In predicting Cys$^-$, the GAT yields Pre/Rec of 0.85/0.47, whereas PROPKA3 fails to predict Cys$^-$.

Surprisingly, the GAT has similar performances as PROPKA3 for His, Lys and Tyr (Figure 5B and D). Although the GAT gives a slightly lower RMSE for His pK_a's, the Pre of predicting His$^+$ is only 0.25, lower than PROKA3's 0.60. Like PROPKA3, the GAT fails to predict Lys^0, and the RMSE for Tyr pK_a's is slightly higher.

Comparison of KaML-CBtree, KaML-GAT, and previous ML models

Performance comparison between KaML-CBtree and KaML-GAT. Both the overall and amino acid specific metrics demonstrate that the CBtree outperforms the GAT (Table 2, Figure 3, Figure 5, and Table 3). Except for His, which shows similar RMSEs between the two models, the CBtree gives lower RMSEs for individual amino acids. Importantly, the CBtree's CERs for all but Asp are substantially reduced compared to the GAT (Table 3).

The performance of both the CBtree and GAT correlates with dataset size: lowest RMSE for Glu (largest dataset) and highest RMSE for Cys/Tyr (smallest datasets). However, besides the significant decrease in RMSEs, the CBtree's CERs for Cys and Lys are reduced by 30% and 65%, respectively, relative to the GAT. This suggests that the CBtree

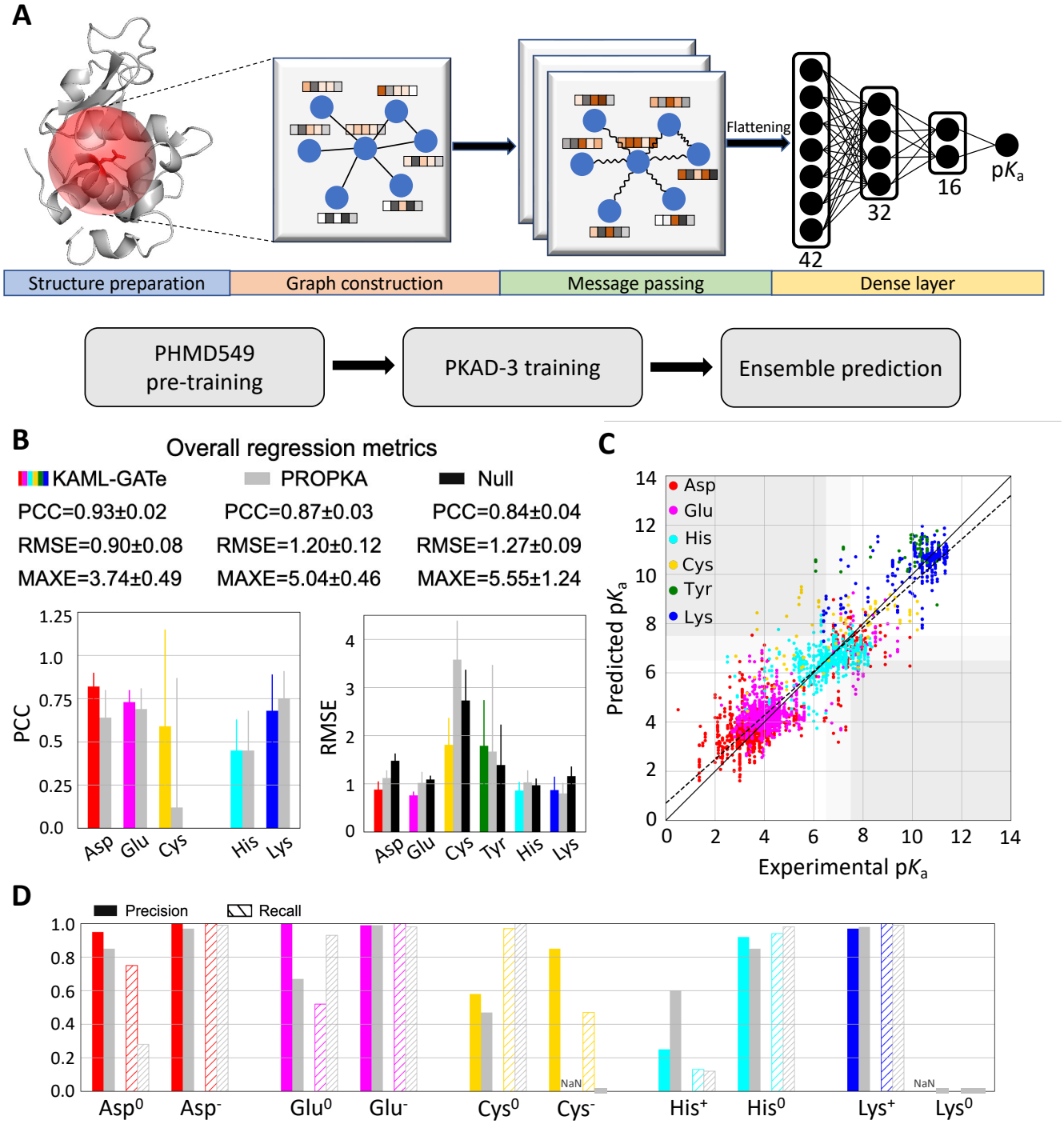

Figure 5: **Schematic of KaML-GAT and its performance of predicting pK_a's and protonation states for five amino acids. A.** Schematic of KaML-GAT architecture (top) and workflow (bottom). **B.** Overall (top) and amino acid specific PCC and RMSE for pK_a predictions by KaML-GAT (colored), PROPKA3 (grey),[15] and null model (black). **C.** The predicted vs. experimental pK_a's from 20 unseen tests. The plots for individual tests are given in SI Figure S5. **D.** Precision (solid) and recall (strips) in predicting protonation states at pH 7 for individual amino acids by KaML-GAT and PROPKA3.

is less sensitive to the dataset size than the GAT.

KaML-CBtree and KaML-GAT share common missteps. Since the CBtree and GAT have distinct algorithms, we asked if they make different errors in the pK_a predictions. To address this question, the model residuals, pK_a(pred)-pK_a(expt), are plotted against each other (Figure 6). For both models, most residuals cluster around zero and spread symmetrically indicating no systematic errors. However, surprisingly, the residuals of the GAT show a high correlation (PCC of 0.73) with those of the CBtree. This indicates that both models produce errors of similar amplitude and of the same sign for most entries in the dataset. Indeed, ensembling CBtree and GAT predictions failed to reduce RMSEs (data not shown).

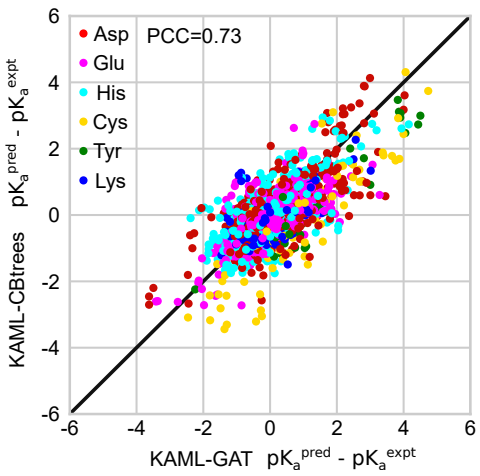

Figure 6: **Model residuals are highly correlated between KaML-CBtree and KaML-GAT.** For every instance in the test sets the residuals (difference between the predicted and experimental pK_a's) of the CBtree and GAT are plotted against each other. The solid line is identity.

Close examination of the largest residuals reveals that both models have difficulty predicting the anomalous pK_a's of mutant SNase. An extreme example is T41D SNase. In the (homology) modeled structure, Asp41 is deeply buried and (accordingly) the predicted pK_a by either GAT or CBtree is ∼8; however, the experimental value is ∼4. Analogously, the deeply buried Lys132 in A132K SNase has an experimental pK_a of 10.4, whereas the CBtree and GAT predict 6.9 and 8.9, respectively. Constant pH MD simulations[47] and experimental evidence[48,49] suggest that the abnormally small pK_a shifts of deeply buried residues is due to partial unfolding and/or water penetration which allows stabilization of the ionized form.

An example where both models fail to recapitulate large experimental pK_a shift is Asp118 in N118D SNase (PDB: 5KGU), which has an experimental pK_a of 7.0 but both the GAT and CBtree predict a pK_a of ∼4.0. Asp118 is in a unique environment: its side-chain is fully buried near positively charged Lys and Arg, while its backbone lies close to the protein surface. We hypothesized that both models overestimate attractive electrostatic contributions stabilizing the charged state; however, the following two examples of large residuals contradict this. Asp75 in barnase (PDB: 1FW7) has an experimental pK_a of 3.1, while the CBtree and GAT predicts 7.3 and 6.5, respectively. Cys48 in glutathione S-transferase (PDB: 5X79) has an experimental pK_a of 3.7, while the CBtree and GAT predicts 7.2 and 8.8, respectively. The microenvironment of Asp75 in barnase and Cys48 in S-transferase share key similarities with Asp118 in N118D SNase: in each case, the titratable side-chain is buried in close proximity to one or two charged side-chains, while the backbone is positioned near the surface. However, the models either under- (Asp118) or overestimate (Asp75 and Cys48) the attractive electrostatics. For edge cases of buried residues in proximity to both solvent and charged side-chains, small conformational changes can significantly alter the local environment of the titratable residue. The effects due to conformational changes are not captured by the ML models.

KaML-CBtree significantly outperforms the PB and alternative ML models. The CBtree outperforms the PB method

Table 3: Performance comparison of KaML-CBtree, KaML-GAT, PB, and alternative ML models[a]

	PypKa		DeepKa		ANI-2X [b]		KaML-CBtree		KaML-GAT	
	RMSE	CER	RMSE	CER	RMSE	CER	RMSE	CER	RMSE	CER
Asp	1.61 ± 0.28	$56/917$	1.23 ± 0.35	$48/937$	1.20 ± 0.14	$52/929$	0.75 ± 0.17	$13/916$	0.88 ± 0.17	$5/901$
Glu	0.86 ± 0.12	$25/1039$	0.84 ± 0.25	$9/1068$	0.81 ± 0.12	$40/1075$	0.60 ± 0.07	$5/1076$	0.76 ± 0.08	$12/1053$
His	1.13 ± 0.51	$8/257$	1.10 ± 0.49	$12/248$	0.52 ± 0.16	$3/298$	0.85 ± 0.14	$11/209$	0.86 ± 0.18	$26/203$
Cys	3.15 ± 0.97	$21/56$	n/a	n/a	n/a	n/a	1.50 ± 0.60	$13/68$	1.81 ± 0.56	$16/59$
Lys	1.01 ± 0.30	$10/325$	0.77 ± 0.25	$2/322$	1.14 ± 0.22	$10/325$	0.70 ± 0.21	$1/325$	0.87 ± 0.28	$8/325$
Tyr	1.49 ± 1.25	-	n/a	n/a	1.88 ± 1.46	-	1.24 ± 0.85	-	1.79 ± 0.95	-

[a]PypKa[12] and ANI-2X[30] predictions were made with the local installed software provided by the authors. DeepKa predictions were obtained from the DeepKa web server.[50] n/a (not available) indicates that the model is unable to make predictions. CER of Tyr is not calculated due to the extremely small test sets (3 Tyr$^-$). [b]Our test sets likely overlap with ANI-2X's training set; removing overlap is impossible as the data in Ref[30] is unpublished.

(PyPKa)[12] and alternative ML models (PKAI, PKAI+,[23] DeepKa[27,51]), when compared to the reported overall metrics (SI Table S9). However, this comparison is not optimal due to the different test sets used. Moreover, the published models[23,27,30,51] were evaluated using only one test set, making a fair comparison even harder. Furthermore, many models ignore Cys and Tyr, e.g. DeepKa,[27,51] which results in underestimation of the overall RMSE since Cys and Tyr are associated with larger errors. To ensure a fair comparison among different models, we used our 20 hold-out test sets to evaluate the amino acid specific metrics for predicting pK_a's and protonation states by PypKa,[12] DeepKa,[27,50] and ANI-2X.[30] Note, our test sets likely overlap with the training data of ANI-2X; however, removing overlap is impossible due to unavailability of data in Ref.[30]

KaML-CBtree's RMSEs and CERs are significantly lower than PypKa and DeepKa for all amino acids (Table 3 and SI Table S10). KaML-CBtree's RMSEs and CERs are also significantly lower than ANI-2X, except for His, for which ANI-2X's RMSE is 0.52. Considering the author reported test RMSE of 0.98 for His[30] and the significantly higher RMSEs of Asp (1.20) and Glu (0.81) in our tests (Asp and Glu were trained using much larger training datasets), we attribute the unexpectedly low RMSE for His to an overlap between our test sets and ANI-2X's training set.

Comparison of KaML-GAT's metrics with those of PypKa and DeepKa shows that KaML-GAT excels at predicting the pK_a's and protonation states of Asp and Cys, while the performance for Glu is similar to DeepKa which surpasses PypKa (Table 3). Interestingly, KaML-GAT's RMSE and CER for Lys are lower than PypKa and ANI-2X, which have similar performances; however, DeepKa's RMSE is 0.1 units and CER is four times lower compared to KaML-GAT. We attribute DeepKa's excellent performance for Lys to the high accuracy of the GBNeck2-CpHMD titration for Lys[5] and its significantly larger training data of downshifted pK_a's as compared to KaML-GAT.

Curiously, although KaML-GAT's RMSE for His is more than 0.24 lower than PypKa and DeepKa, the CER is respectively 3.2 and 2.2 times (Table 3). This performance is related to KaML-GAT's low Pre and Rec for predicting His$^+$ (Figure 5D). The largest residuals for PypKa are from either overestimating extremely low experimental p$K_a$values or underestimating experimental p$K_a$values around 6.0. Those instances lead to an increased RMSE without affecting the CER.

Concluding Discussion

We developed the shallow decision tree (KaML-CBtree) and deep learning (KaML-GAT) models to predict pK_a's and protonation states of all six titratable amino acids based on a newly curated, significantly expanded experimental pK_a database PKAD-3. While both KaML-CBtree and KaML-GAT outper-

form PROPKA3, KaML-CBtree offers more accurate pK_a and protonation state predictions for all six titratable amino acids. KaML-CBtree's RMSEs and CERs are also significantly lower than the PB method (PypKa) and ML models trained on the state-of-the-art GBNeck2-CpHMD pK_a's (DeepKa)[27,50] and atom-centered quantum potential energies (ANI-2X).[30] Perhaps the most significant improvement over previous models is the model's capability of accurately predicting Asp^0, Glu^0, Cys^-, and Lys^0, which often play important roles in biological functions. In contrast, previous models either fail or are incapable of making predictions. For Asp^0, PypKa, ANI-2X, and DeepKa yield Rec of 0, 0.09, and 0.12 respectively. For Glu^0, PypKa and ANI-2X yield Rec of 0.24 and 0, respectively. While ANI-2X and DeepKa are not trained to make predictions for Cys, PypKa gives Rec of 0.16 for Cys^-. Neither ANI-2X nor PypKa predicts any Lys^0, i.e. Rec of 0.

One surprising finding is that the performance of the KaML-CBtree well surpasses KaML-GAT, despite having two orders of magnitude smaller parameter space ($\sim$8,000 for GAT). Decision trees benefit from simplicity and interpretability, which can lead to more efficient training and better model generalization. Deep learning models are potentially more accurate but require much larger training dataset. The impact of dataset size is evident in KaML-GAT's performance improvement with the AF2 data augmentation (data not shown), while KaML-CBtree shows no such sensitivity (SI Table S11). Two recent studies[52,53] found that regularity, i.e., feature distributions that are less skewed and less heavy-tailed, is predictive of neural networks outperforming gradient-boosted tree models for tabular data. Thus, we hypothesized that, in addition to the small dataset, the higher performance of KaML-CBtree may be attributed to the irregularity of features. McElfresh et al.[53] introduced a feature irregularity parameter as a linear function of specific meta features. Using a large number of datasets and models, they found[53] that the feature irregularity score ranges from 0 to 7 and tree models outperform neural networks when the irregularity score is greater than 5. When calculating the feature irregularity score using the tree features of the entire dataset, we obtained a value of 6.3, which suggests highly irregular features, thus providing a rationale for why KaML-CBtree outperforms KaML-GAT. On the other hand, the lower performance of KaML-GAT may also be attributed to the limitations of the pre-training data, especially the PHMD549 dataset's exclusion of Cys and Tyr. This can be seen from the significantly higher RMSEs of Cys and Tyr pK_a's as compared to those of KaML-CBtree.

The present models have several other limitations. The training and testing datasets for Tyr and Cys are extremely small, leading to larger prediction errors and potentially unreliable model evaluation metrics. Another challenge is related to the class imbalance between protonated and deprotonated states, which reduces the prediction accuracy for the minority class. For this reason, the recall of His^+ is significantly lower than any other amino acid's minority protonation state. In our current evaluation of regression models' classification power, the titrating class is excluded. This leads to an incomplete picture of model performance, particularly for His, as the most probable experimental pK_a's are near 7. Furthermore, in some applications, the ability to accurately identify titrating residues is crucial for understanding pH-dependent behavior. Despite these limitations, KaML-CBtree demonstrates promising accuracy and precision for predicting protein electrostatics. To enable applications and facilitate further development in the community, we release PKAD-3 and an end-to-end pK_a prediction tool based on KaML-CBtree.

Acknowledgment

Financial support by the National Institutes of Health (R35GM148261 and R01CA256557) is acknowledged. We thank Dr. Guy Dayhoff for providing a command line version of the protein disorder prediction tool RIDAO.[54]

Data Availability

The PKAD-3 database is freely searchable and downloadable at `https://database.computchem.org/pkad3`. All training and test sets, the 20 CBtree and GAT models, the final CBtree model for deployment, as well as and the Python program for calculating tree features are freely downloadable at `https://github.com/JanaShenLab/KaMLs/`.

Supporting Information Available

Supporting Information contains Materials and Methods as well as supplementary tables and figures. Table S1 contains description of features of tree models. Table S2 and S3 list regression and classification metrics for the different KaML-trees, respectively. Table S4 and S5 list amino acid specific regression and classifications metrics for KaML-CBtrees and PROPKA3, respectively. Table S6 gives atom types for KaML-GATs. Table S7 lists regression metrics for the different freezing schemes for KaML-GATs. Table S8 lists amino acid specific regression and classifications metrics for KaML-GAT. Table S9 gives the author-reported regression metrics for the published pK_a prediction methods. Table S10 gives regression metrics from the previous ML models evaluated on our test sets. Figure S1 shows the pK_a distributions and train test splits. Figure S2 shows t-SNE plot at pH 7.5 Figure S3 and S5 show predicted vs experimental pK_a values for all 20 test sets for KaML-CB and KaML-GAT, respectively. Figure S4 shows the training and validation loss of KaML-GAT. Figure S6 shows the dependence of ensemble GAT on the number of models in the ensemble.

References

(1) Huang, Y.; Yue, Z.; Tsai, C.-C.; Henderson, J. A.; Shen, J. Predicting Catalytic Proton Donors and Nucleophiles in Enzymes: How Adding Dynamics Helps Elucidate the Structure-Function Relationships. *J. Phys. Chem. Lett.* **2018**, *9*, 1179–1184.

(2) DeCoursey, T. E. Voltage and pH Sensing by the Voltage-Gated Proton Channel, HV1. *J. R. Soc. Interface* **2018**, *15*, 20180108.

(3) Drew, D.; Boudker, O. Ion and Lipid Orchestration of Secondary Active Transport. *Nature* **2024**, *626*, 963–974.

(4) Roos, G.; Foloppe, N.; Messens, J. Understanding the p K_a of Redox Cysteines: The Key Role of Hydrogen Bonding. *Antioxid. Redox Signal.* **2013**, *18*, 94–127.

(5) Liu, R.; Yue, Z.; Tsai, C.-C.; Shen, J. Assessing Lysine and Cysteine Reactivities for Designing Targeted Covalent Kinase Inhibitors. *J. Am. Chem. Soc.* **2019**, *141*, 6553–6560.

(6) Webb, H.; Tynan-Connolly, B. M.; Lee, G. M.; Farrell, D.; O'Meara, F.; Søndergaard, C. R.; Teilum, K.; Hewage, C.; McIntosh, L. P.; Nielsen, J. E. Remeasuring HEWL pKa Values by NMR Spectroscopy: Methods, Analysis, Accuracy, and Implications for Theoretical pKa Calculations. *Proteins* **2011**, *79*, 685–702.

(7) Alexov, E.; Mehler, E. L.; Baker, N.; M. Baptista, A.; Huang, Y.; Milletti, F.; Erik Nielsen, J.; Farrell, D.; Carstensen, T.; Olsson, M. H. M.; Shen, J. K.; Warwicker, J.; Williams, S.; Word, J. M. Progress in the Prediction of pKa Values in Proteins. *Proteins* **2011**, *79*, 3260–3275.

(8) Anandakrishnan, R.; Aguilar, B.; Onufriev, A. V. H++ 3.0: Automating pK Prediction and the Preparation of Biomolecular Structures for Atomistic Molecular Modeling and Simulations.

Nucl. Acids Res. **2012**, *40*, W537–W541.

(9) Pahari, S.; Sun, L.; Basu, S.; Alexov, E. DelPhiPKa: Including Salt in the Calculations and Enabling Polar Residues to Titrate. *Proteins* **2018**, *86*, 1277–1283.

(10) Dolinsky, T. J.; Nielsen, J. E.; McCammon, J. A.; Baker, N. A. PDB2PQR: An Automated Pipeline for the Setup of Poisson-Boltzmann Electrostatics Calculations. *Nucleic Acids Res.* **2004**, *32*, W665–W667.

(11) Song, Y.; Mao, J.; Gunner, M. R. MCCE2: Improving Protein p K_a Calculations with Extensive Side Chain Rotamer Sampling. *J. Comput. Chem.* **2009**, NA–NA.

(12) Reis, P. B. P. S.; Vila-Viçosa, D.; Rocchia, W.; Machuqueiro, M. PypKa: A Flexible Python Module for Poisson–Boltzmann-Based pKa Calculations. *J. Chem. Inf. Model.* **2020**, *60*, 4442–4448.

(13) Schutz, C. N.; Warshel, A. What Are the Dielectric "Constants" of Proteins and How to Validate Electrostatic Models? *Proteins* **2001**, *44*, 400–417.

(14) Li, H.; Robertson, A. D.; Jensen, J. H. Very Fast Empirical Prediction and Rationalization of Protein pKa Values. *Proteins* **2005**, *61*, 704–721.

(15) Olsson, M. H. M.; Søndergaard, C. R.; Rostkowski, M.; Jensen, J. H. PROPKA3: Consistent Treatment of Internal and Surface Residues in Empirical p K_a Predictions. *J. Chem. Theory Comput.* **2011**, *7*, 525–537.

(16) Martins de Oliveira, V.; Liu, R.; Shen, J. Constant pH Molecular Dynamics Simulations: Current Status and Recent Applications. *Curr. Opin. Struct. Biol.* **2022**, *77*, 102498.

(17) Harris, R. C.; Liu, R.; Shen, J. Predicting Reactive Cysteines with Implicit-Solvent-Based Continuous Constant pH Molecular Dynamics in Amber. *J. Chem. Theory Comput.* **2020**, *16*, 3689–3698.

(18) Harris, J. A.; Liu, R.; Martins de Oliveira, V.; Vázquez-Montelongo, E. A.; Henderson, J. A.; Shen, J. GPU-Accelerated All-Atom Particle-Mesh Ewald Continuous Constant pH Molecular Dynamics in Amber. *J. Chem. Theory Comput.* **2022**, *18*, 7510–7527.

(19) Pahari, S.; Sun, L.; Alexov, E. PKAD: A Database of Experimentally Measured pKa Values of Ionizable Groups in Proteins. *DATABASE* **2019**, *2019*.

(20) Ancona, N.; Bastola, A.; Alexov, E. PKAD-2: New Entries and Expansion of Functionalities of the Database of Experimentally Measured pKa's of Proteins. *J. Comput. Biophys. Chem.* **2023**, 1–10.

(21) Reis, P. B. P. S.; Clevert, D.-A.; Machuqueiro, M. pKPDB: A Protein Data Bank Extension Database of p *Ka* and pI Theoretical Values. *Bioinformatics* **2021**, *38*, 297–298.

(22) Rocchia, W.; Alexov, E.; Honig, B. Extending the Applicability of the Nonlinear Poisson-Boltzmann Equation: Multiple Dielectric Constants and Multivalent Ions. *J. Phys. Chem. B* **2001**, *105*, 6507–6514.

(23) Reis, P. B.; Bertolini, M.; Montanari, F.; Rocchia, W.; Machuqueiro, M.; Clevert, D.-A. A Fast and Interpretable Deep Learning Approach for Accurate Electrostatics-Driven p K_a Predictions in Proteins. *J. Chem. Theory Comput.* **2022**, *18*, 5068–5078.

(24) Wallace, J. A.; Shen, J. K. Continuous Constant pH Molecular Dynamics in Explicit Solvent with pH-Based Replica Exchange. *J. Chem. Theory Comput.* **2011**, *7*, 2617–2629.

(25) Huang, Y.; Harris, R. C.; Shen, J. Generalized Born Based Continuous Constant pH Molecular Dynamics in Amber: Implementation, Benchmarking and Analysis. *J. Chem. Inf. Model.* **2018**, *58*, 1372–1383.

(26) Harris, R. C.; Shen, J. GPU-Accelerated Implementation of Continuous Constant pH Molecular Dynamics in Amber: pKa Predictions with Single-pH Simulations. *J. Chem. Inf. Model.* **2019**, *59*, 4821–4832.

(27) Cai, Z.; Liu, T.; Lin, Q.; He, J.; Lei, X.; Luo, F.; Huang, Y. Basis for Accurate Protein p K_a Prediction with Machine Learning. *J. Chem. Inf. Model.* **2023**, *63*, 2936–2947.

(28) Chen, A. Y.; Lee, J.; Damjanovic, A.; Brooks, B. R. Protein pKa Prediction by Tree-Based Machine Learning. *J. Chem. Theory Comput.* **2022**,

(29) Liu, S.; Yang, Q.; Zhang, L.; Luo, S. Accurate Protein pKa Prediction with Physical Organic Chemistry Guided 3D Protein Representation. *J. Chem. Inf. Model.* **2024**, *64*, 4410–4418.

(30) Gokcan, H.; Isayev, O. Prediction of Protein p K_a with Representation Learning. *Chem. Sci.* **2022**, *13*, 2462–2474.

(31) Veličković, P.; Cucurull, G.; Casanova, A.; Romero, A.; Liò, P.; Bengio, Y. Graph Attention Networks. 2018.

(32) Jumper, J. et al. Highly Accurate Protein Structure Prediction with AlphaFold. *Nature* **2021**, *596*, 583–589.

(33) Marino, S. M.; Gladyshev, V. N. Analysis and Functional Prediction of Reactive Cysteine Residues. *J. Biol. Chem.* **2012**, *287*, 4419–4425.

(34) Isom, D. G.; Cannon, B. R.; Castañeda, C. A.; Robinson, A.; García-Moreno E., B. High Tolerance for Ionizable Residues in the Hydrophobic Interior of Proteins. *Proc. Natl. Acad. Sci. USA* **2008**, *105*, 17784–17788.

(35) Castañeda, C. A.; Fitch, C. A.; Majumdar, A.; Khangulov, V.; Schlessman, J. L.; García-Moreno, B. E. Molecular Determinants of the p K_a Values of Asp and Glu Residues in Staphylococcal Nuclease: p K_a Values of Asp and Glu in SNase. *Proteins* **2009**, *77*, 570–588.

(36) Isom, D. G.; Castañeda, C. A.; Cannon, B. R.; Velu, P. D.; García-Moreno E., B. Charges in the Hydrophobic Interior of Proteins. *Proc. Natl. Acad. Sci. U.S.A.* **2010**, *107*, 16096–16100.

(37) Isom, D. G.; Castaneda, C. A.; Cannon, B. R.; Garcia-Moreno E., B. Large Shifts in pKa Values of Lysine Residues Buried inside a Protein. *Proc. Natl. Acad. Sci. USA* **2011**, *108*, 5260–5265.

(38) Kougentakis, C. M.; Grasso, E. M.; Robinson, A. C.; Caro, J. A.; Schlessman, J. L.; Majumdar, A.; García-Moreno E., B. Anomalous Properties of Lys Residues Buried in the Hydrophobic Interior of a Protein Revealed with ^{15}N-Detect NMR Spectroscopy. *J. Phys. Chem. Lett.* **2018**, *9*, 383–387.

(39) Shi, C.; Wallace, J. A.; Shen, J. K. Thermodynamic Coupling of Protonation and Conformational Equilibria in Proteins: Theory and Simulation. *Biophys. J.* **2012**, *102*, 1590–1597.

(40) Liu, R.; Clayton, J.; Shen, M.; Bhatnagar, S.; Shen, J. Machine Learning Models to Interrogate Proteome-Wide Covalent Ligandabilities Directed at Cysteines. *JACS Au* **2024**, *4*, 1374–1384.

(41) Wallace, J. A.; Shen, J. K. *Methods Enzymol.*; Elsevier, 2009; Vol. 466; pp 455–475.

(42) Hinton, G. E.; Roweis, S. Stochastic Neighbor Embedding. Adv Neur Inf. Process Sys. 2002.

(43) van der Maaten, L.; Hinton, G. Visualizing Data Using T-SNE. *J. Mach. Learn. Res.* **2008**, *9*, 2579–2605.

(44) Thurlkill, R. L.; Grimsley, G. R.; Scholtz, J. M.; Pace, C. N. pK Values of the Ionizable Groups of Proteins. *Protein Sci.* **2006**, *15*, 1214–1218.

(45) Lundberg, S. M.; Lee, S.-I. A Unified Approach to Interpreting Model Predictions. Adv. Neural Inf. Process. Syst. 2017; pp 4768–4777.

(46) Polikar, R. Ensemble Based Systems in Decision Making. *IEEE Circuits Syst. Mag.* **2006**, *6*, 21–45.

(47) Wallace, J. A.; Wang, Y.; Shi, C.; Pastoor, K. J.; Nguyen, B.-L.; Xia, K.; Shen, J. K. Toward Accurate Prediction of pKa Values for Internal Protein Residues: The Importance of Conformational Relaxation and Desolvation Energy. *Proteins* **2011**, *79*, 3364–3373.

(48) Harms, M. J.; Schlessman, J. L.; Chimenti, M. S.; Sue, G. R.; Damjanović, A.; García-Moreno E., B. A Buried Lysine That Titrates with a Normal pKa: Role of Conformational Flexibility at the Protein-Water Interface as a Determinant of pKavalues. *Protein Sci.* **2008**, *17*, 833–845.

(49) Peck, M. T.; Ortega, G.; De Luca-Johnson, J. N.; Schlessman, J. L.; Robinson, A. C.; García-Moreno E, B. Local Backbone Flexibility as a Determinant of the Apparent p K_a Values of Buried Ionizable Groups in Proteins. *Biochemistry* **2017**, *56*, 5338–5346.

(50) Cai, Z.; Peng, H.; Sun, S.; He, J.; Luo, F.; Huang, Y. DeepKa Web Server: High-Throughput Protein p K_a Prediction. *Journal of Chemical Information and Modeling* **2024**, *64*, 2933–2940.

(51) Cai, Z.; Luo, F.; Wang, Y.; Li, E.; Huang, Y. Protein p K_a Prediction with Machine Learning. *ACS Omega* **2021**, *6*, 34823–34831.

(52) Grinsztajn, L.; Oyallon, E.; Varoquaux, G. Why Do Tree-Based Models Still Outperform Deep Learning on Typical Tabular Data? 36th Conference on Neural Information Processing Systems. 2022.

(53) McElfresh, D.; Khandagale, S.; Valverde, J.; Feuer, B.; Hegde, C.; Ramakrishnan, G.; Goldblum, M.; White, C. When Do Neural Nets Outperform Boosted Trees on Tabular Data? 37th Conference on Neural Information Processing Systems. 2023.

(54) Dayhoff II, G. W.; Uversky, V. N. Rapid Prediction and Analysis of Protein Intrinsic Disorder. *Protein Sci.* **2022**, *31*, e4496.